REVERSE-TIME MIGRATION AND FULL WAVEFROM INVERSION APPLIED TO A STATIONARY MIMO GPR SYSTEM

Hai Liu[1], Yuxian Zhang[1], Chen Qiu[1], Feng Han[1], Qing Huo Liu[1, 2]*

[1] Institute of Electromagnetics Acoustics, and Department of Electronic Science, Xiamen University, Xiamen, 361005, China.
[2] Department of Electrical and Computer Engineering, Duke University, Durham, NC 27708, USA.

[*]Corresponding email: liuhai8619@xmu.edu.cn

ABSTRACT

This paper presents a multi-input and multi-output (MIMO) ground penetrating radar (GPR) system, which is going to be launched to the moon for imaging shallow regolith structures and estimating the dielectric properties. This system, as an important part of China' Chang-E 5 lunar exploration mission, employs twelve off-ground Vivaldi antennas as transmitters/receivers, and works in a stationary mode. A reverse-time migration algorithm is developed to process the MIMO GPR dataset for obtaining a high-resolution image of the subsurface objects. The results of a laboratory experiment on a volcanic ash pit demonstrate that the upper and lower interfaces of a marble slab of 3 cm thickness buried at a depth up to 2 m can be clearly imaged. A full waveform inversion algorithm based on Born iterative method is applied to invert the dielectric properties of the subsurface objects. The preliminary results of a numerical experiment demonstrate that the dielectric permittivity of a subsurface cubic object can be accurately obtained using the MIMO GPR dataset at only six discrete frequencies.

Index Terms — ground-penetrating radar (GPR), multi-input and multi-output (MIMO), reverse time migration (RTM), full waveform inversion (FWI), lunar exploration

1. INTRODUCTION

As a promising non-destructive detection and imaging tool, ground-penetrating radar (GPR) has been popularly applied in various fields [1]–[3]. Conventionally, a GPR system employs a pair of antennas for transmitting and receiving electromagnetic waves and moves along a survey line, acquiring dense discrete data. A synthetic aperture radar (SAR) algorithm is commonly used to process the common-offset GPR data and to improve the lateral imaging resolution [4][5][7]. Compared with a conventional single-channel GPR system, a GPR system with a multi-input and multi-output (MIMO) antenna array is not only more efficient in 3D data acquisition, but also allows collecting a multi-offset dataset, thereby providing additional information for a more effective subsurface imaging and detection [8].

A MIMO GPR system is going to be launched to the moon by the China's Chang-E 5 lunar exploration mission in 2017. This system is equipped with twelve off-ground Vivaldi antennas, one of which is sequentially used as a transmitter and the other eleven receive the radar echoes at a height of about 90 cm above the ground surface. But unlike a normal GPR system, this MIMO GPR system works in a stationary mode. We have to image the lunar regolith structure and estimate the dielectric properties of the lunar soil and rock from the total 132 radar echoes.

To obtain a high-resolution image of the lunar regolith structures, we developed a reverse time migration algorithm. The principle is presented in the second section and the results of both numerical and laboratory experiments are shown in the third section. To inverse the dielectric properties of the buried object in lunar soil, we applied a full waveform inversion scheme base on Born iterative method to the MIMO GPR dataset. The next section briefly introduce its theory and the preliminary results of a numerical experiment are given in the fourth section. The conclusion is given in the last section.

2. METHODOLOGY OF FDTD

2.1. RTM algorithm

RTM is a recently developed algorithm for imaging the geological structures in seismic exploration. We apply it to process the MIMO GPR dataset and the principle of a 2D RTM algorithm is briefly given by

$$I(x,z) = \sum_m \sum_n T_m(n\Delta t, x, z) R_m(n\Delta t, x, z) \qquad (1)$$

where $T_m(n\Delta t, x, z)$ is the electromagnetic field distribution radiated from the m-th transmiting antenna at the n-th time

step, and $R_m(n\Delta t, z, x)$ the back-propagated field from the recorded field by the eleven receiving antennas, $I(x, z)$ is the RTM image, m is the number of the transmitting antenna and n is the number of time step.

We use cross-correlation as the imaging condition. Finite element time domain (FDTD) method is used to solve the Maxwell equation and calculate the wave fields for RTM.

2.2. FWI algorithm

The dielectric properties of a 3D object buried in the layered medium is reconstructed by a FWI algorithm based on the Born iterative method (BIM) [9]. A cost function $F(\chi)$ is defined as

$$F(\chi) = \| \mathbf{f} - [L]\chi \| + \gamma^2 \| \chi \|^2 \qquad (2)$$

where $\mathbf{f}$ is the measured scattered field data and γ is the regularization factor. In each BIM inverse iteration, the forward algorithm stabilized biconjugate-gradient fast Fourier transform method (BCGS-FFT) is adopted to calculate the total field in the inverse domain [10]. The $[L]$ operator in the BIM method includes the solved total field effects, and $[L]\chi$ is the predicted scattered field in each inverse iteration. Since the total field solved by BCGS-FFT depends on the contrast χ, the operator $[L]$ also depends on χ. Therefore, minimization of the cost function $F(\chi)$ is a nonlinear problem. This problem is linearized using Born approximation. At each $(n+1)$ iteration, we already know the contrast χ and the total field values from last step, i.e. the n-th step, and can approximate $[L]=[L]n$. Thus, the contrast χ in the inverse domain can be obtained by minimizing the normalized equation defined as

$$F_{n+1} = \frac{\| \mathbf{f} - [L]_n \chi_{n+1} \|^2}{\| \mathbf{f} \|^2} + \gamma^2 \frac{\| \chi_{n+1} \|^2}{\| \chi_n \|^2} \qquad (3)$$

This linear least square problem is equivalent to

$$\left([L]^\dagger [L]_n + \frac{\gamma^2 \| \mathbf{f}^2 \|}{\| \chi_n \|^2} \mathbf{I} \right) \chi_{n+1} = [L]^\dagger \mathbf{f} \qquad (4)$$

3. RESULTS OF 2D RTM

Since two of the twelve antennas are out of the imaging plane, only ten antennas are used in the 2D RTM algorithm. The layout the ten antennas is shown in Fig. 1. This section show the results of a numerical experiments and a laboratory test. An initial model required by the FDTD simulation in RTM is shown in Fig. 1. The relative dielectric permittivity and electric conductivity of the lunar soil are respectively set to be 2.5 and 0.01 mS/m. Since no prior information about

the regolith structure and the buried objects could be obtain, a half-space initial model is employed for the 2D RTM.
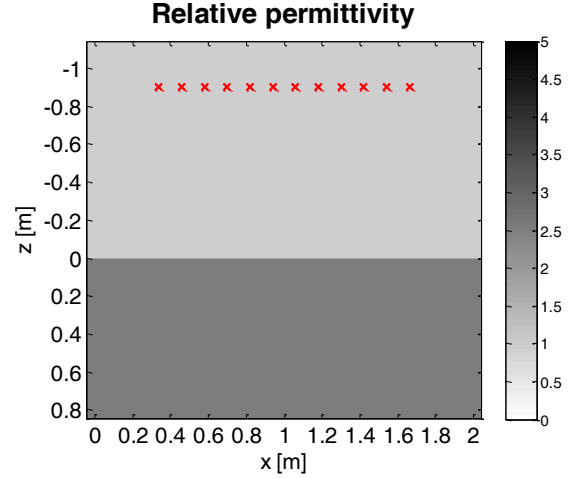
Relative permittivity

Fig. 1 Initial model used for the 2D RTM. The colorbar indicates the dielectric permittivity and the symbol of cross denotes the position of ten antennas.

3.1. A numerical experiment

Fig. 2 shows a 2D model of a numerical experiment. Two 5 cm in diameter cylinder rock are buried at a depth of 50 cm in lunar soil. Ten FDTD simulations are run to produce the MIMO GPR dataset. From the simulated dataset, the RTM image is shown in Fig. 3. We can clearly identify the two objects. The horizontal resolution is also analyzed and the results is given in Fig. 4. The horizontal resolution is about 10 cm at a 50 cm depth and linearly increases with depth.
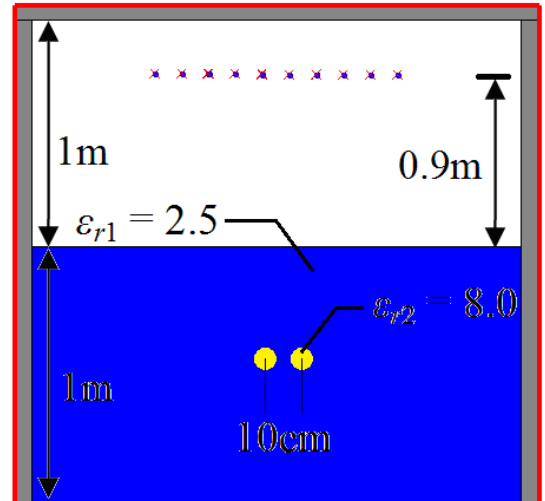

Fig. 2 Geometry of a 2D simulation model. The colorbar indicates the dielectric permittivity and the symbol of cross denotes the position of ten antennas.
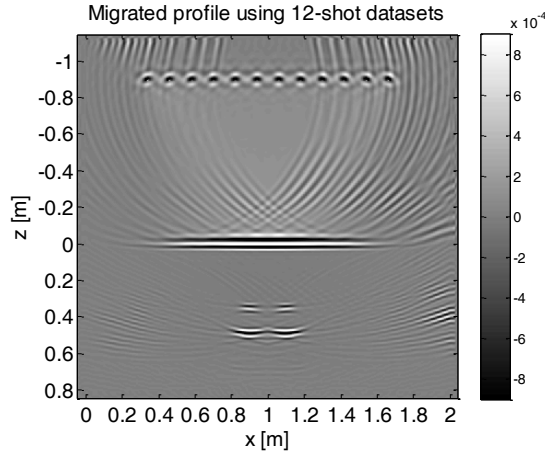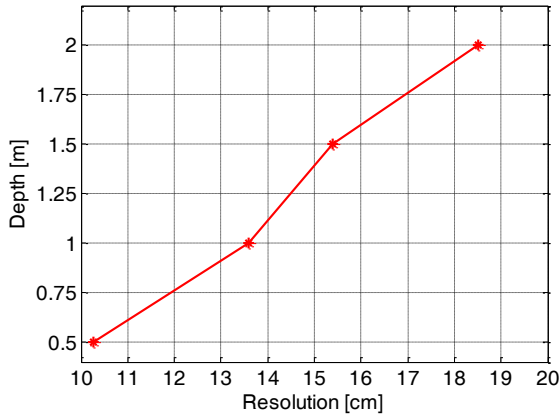
Fig. 3 The 2D-RTM image of the numerical dataset

Fig. 4 Estimated horizontal resolution of the MIMO GPR system

3.2. A laboratory experiment

In the laboratory, we buried three marble slabs at depths of 1 m, 1.5 m and 2 m respectively in a volcanic ash pit, as shown in Fig. 5. The dielectric properties of the volcanic ash are close to those of lunar soil. The relative dielectric permittivity is about 2.5 and the electric conductivity is negligibly small. The thickness and relative dielectric permittivity of the marble slab are 3cm and about 8, respectively. At a depth of 2.5 m, e.g. the bottom of the ash pit, there is a metal plate. Fig. 6 shows the RTM results of the three marble slabs. We can identify the upper and lower interfaces of the slabs, although they are only 3 cm in thickness. This means that the MIMO GPR system has a depth resolution better than 3 cm in marble rock. Considering the velocity difference in marble and lunar soil, we can conclude that the MIMO GPR system has a depth resolution of about 5 cm in lunar soil.
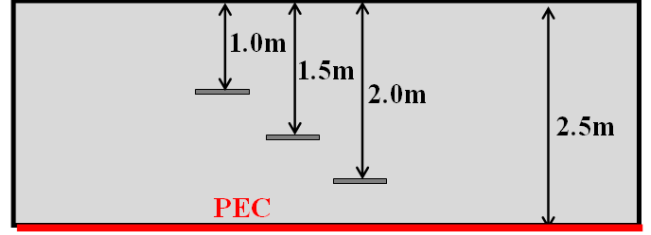

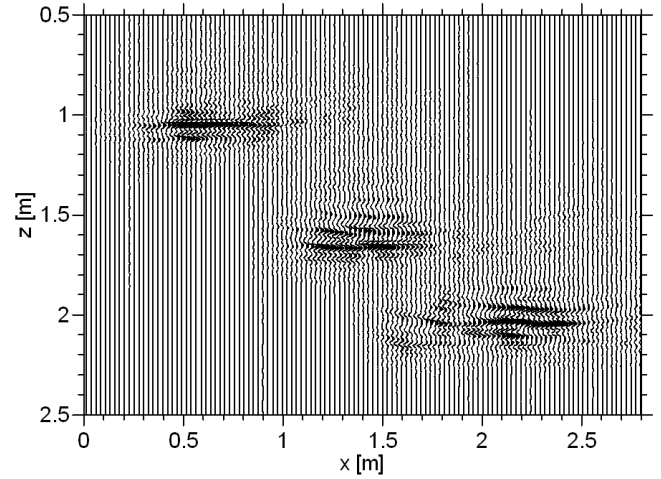Fig. 5 Schematic diagram of the laboratory test.

Fig. 6 The RTM results of the laboratory experiment.

4. PRELIMINARY RESULTS OF FWI

Fig. 7 shows a half space model for FWI. The space above ground surface is air and that in subsurface is lunar soil, of which the dielectric permittivity if 2.5. The source position is located at the twelfth antenna. The target is a 5 cm cubic stone, of which the dielectric permittivity is 4. As demonstrated in the previous section, the subsurface target can be imaged by RTM. A prior information on the target position can be obtained. Thus, we restrict the inversion domain in the red region in Fig. 7. Fig. 8 shows the reconstructed image of dielectric permittivity distribution in the inversion domain using the frequency-domain MIMO GPR dataset at only six discrete frequencies. We can see that the dielectric permittivity of both the lunar soil and the target rock are accurately inverted. However, the cubic rock is imaged to be a sphere shape.
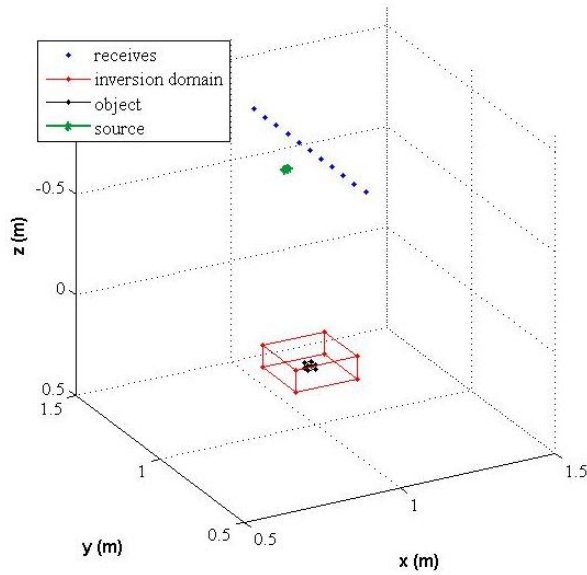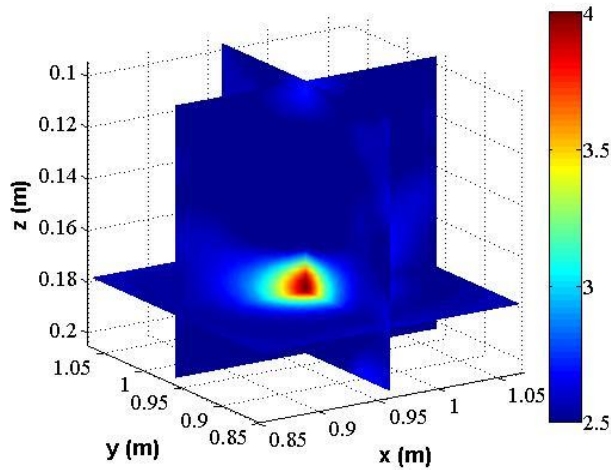
Fig. 7 3D FWI model

Fig. 8 FWI Results of the model in Fig. 7. The color bar indicates the relative dielectric permittivity.

5. CONCLUSION

In this paper, we introduces a stationary MIMO GPR system for shallow lunar exploration. To obtain a high-resolution subsurface image from the MIMO GPR dataset, a 2D RTM algorithm is developed and verified by both numerical and laboratory experiments. The horizontal resolution is about 10 cm at a 50 cm depth and increases with depth. The depth resolution is verified to less than 5 cm in lunar soil and 3 cm in lunar rock. A BIM based FWI algorithm is applied to invert the dielectric properties of the subsurface objects. A numerical experiment demonstrates that the dielectric permittivity of both the lunar soil and target rock can be accurately estimated from the MIMO GPR dataset at only six discrete frequencies. Further research would be conducted to test and improve the FWI algorithm on real data from laboratory experiment.

7. ACKNOWLEDGEMENT

8. REFERENCES

[1] H. Liu and M. Sato, "In situ measurement of pavement thickness and dielectric permittivity by GPR using an antenna array," NDT E Int., no. 64, pp. 65–71, Jun. 2014.

[2] H. Liu, K. Takahashi, and M. Sato, "Measurement of Dielectric Permittivity and Thickness of Snow and Ice on a Brackish Lagoon Using GPR," IEEE J. Sel. Top. Appl. Earth Obs. Remote Sens., vol. 7, no. 3, pp. 820–827, Mar. 2014.

[3] H. Liu, X. Xie, J. Cui, K. Takahashi, and M. Sato, "Groundwater Level Monitoring for Hydraulic Characterization of an Unconfined Aquifer by Common Mid-point Measurements using GPR," J. Environ. Eng. Geophys., vol. 19, no. 4, pp. 259–268, 2014.

[4] L. Xiao, P. Zhu, G. Fang, Z. Xiao, Y. Zou, J. Zhao, Y. Yuan, L. Qiao, X. Zhang, H. Zhang, J. Wang, J. Huang, Q. Huang, Q. He, B. Zhou, Y. Ji, Q. Zhang, S. Shen, Y. Li, and Y. Gao, "A young multilayered terrane of the northern Mare Imbrium revealed by Chang'E-3 mission," Science (80-.)., vol. 347, no. 6227, pp. 1226–1230, 2015.

[5] J. I. Halman, K. A. Shubert, and G. T. Ruck, "SAR processing of ground-penetrating radar data for buried UXO detection: results from a surface-based system," IEEE Trans. Antennas Propag., vol. 46, no. 7, pp. 1023 –1027, 1998.

[6] K. Gu, G. Wang, and J. Li, "Migration based SAR imaging for ground penetrating radar systems," Radar, Sonar Navig. IEE Proc. -, vol. 151, no. 5, pp. 317 – 325, Oct. 2004.

[7] X. Feng, Y. Yu, C. Liu, and M. Fehler, "Combination of H-Alpha Decomposition and Migration for Enhancing Subsurface Target Classification of GPR," IEEE Trans. Geosci. Remote Sens., vol. 53, no. 9, pp. 4852–4861, 2015.

[8] Z. Zeng, J. Li, L. Huang, X. Feng, and F. Liu, "Improving target detection accuracy based on multipolarization MIMO GPR," IEEE Trans. Geosci. Remote Sens., vol. 53, no. 1, pp. 15–24, 2015.

[9] C. Yu, S. Member, M. Yuan, Y. Zhang, J. Stang, R. T. George, G. A. Ybarra, W. T. Joines, and Q. H. Liu, "Microwave Imaging in Layered Media : 3-D Image Reconstruction From Experimental Data," IEEE Trans. Antennas Propag., vol. 58, no. 2, pp. 440–448, 2010.

[10] X. Millard, Q. H. Liu, and S. Member, "Simulation of Near-Surface Detection of Objects in Layered Media by the BCGS – FFT Method," IEEE Trans. Geosci. Remote Sens., vol. 42, no. 2, pp. 327–334, 2004.